Available online at www.sciencedirect.com
ScienceDirect
Journal of Non-Crystalline Solids 354 (2008) 607–611
JOURNAL OF NON-CRYSTALLINE SOLIDS
www.elsevier.com/locate/jnoncrysol

Formation of nanoparticles in soda-lime glasses by single and double ion implantation

M. Dubiel [a,*], H. Hofmeister [b], E. Wendler [c]

[a] Martin Luther University of Halle-Wittenberg, Institute of Physics, Friedemann-Bach-Platz 6, D-06108 Halle, Germany
[b] Max Planck Institute of Microstructure Physics, Weinberg 2, D-06120 Halle, Germany
[c] Institute of Solid State Physics, University of Jena, D-07743 Jena, Germany

Available online 14 November 2007

Abstract

Structural characteristics and optical properties of monometallic and bimetallic Ag and Au nanoparticles in the surface region of soda-lime glass fabricated by ion implantation have been studied by transmission electron microscopy and optical spectroscopy. As a result it has been found that both, implantation dose and process temperature, strongly influence the metal nanoparticle formation governed by ion diffusion and metal precipitation as well as the involved stress generation around the particles. Thus, the mean size of metal nanoparticles and the width of the particle containing region beneath the glass surface increase with increasing temperature as well as implanted dose. Upon sequential high-dose double implantation to form bimetallic Ag–Au nanoparticles a rather complex configuration has been obtained. Particles of sizes above a threshold of 5–10 nm exhibit distinct image contrast features indicating the development of central voids whose sizes are proportional to the outer particle diameter.

PACS: 61.80.−x; 61.16.−d; 61.46.+w

Keywords: Alloys; Nanocrystals; Optical spectroscopy; STEM/TEM; TEM/STEM; Nano-composites; Nanoparticles; Soda-lime-silica

1. Introduction

Metal nanoparticles embedded in glass have been thoroughly studied because of their optical properties and potential technical applications [1–4]. There are a number of methods currently used for the fabrication of such composite materials. One of them, namely ion implantation, enables to introduce high concentrations as well as different metals into surface-near regions of the glass. This way, specific linear and non-linear optical properties have been achieved, especially, for Au, Ag or Cu nanoparticles in silica glasses, see for example [5–7].

Recently, the preparation of bimetallic nanoparticles has been intensively investigated because of the far-reaching possibilities to modify the macroscopic properties, e.g. the optical absorption and chemical reactivity, of such materials. Studies on Ag–Au nanoparticles are typically concerned with the issues of separated monometallic particles, segregated bimetallic particles, and alloy particles [8–11]. Some work has been done dealing with the formation of bimetallic or alloy nanoparticles by double ion implantation in silica glass [12–15] where the existence of such particles, their structure and thermal stability have been explored using optical spectroscopy, transmission electron microscopy (TEM), X-ray absorption fine structure (EXAFS) spectroscopy as well as of X-ray diffraction and scattering.

The present work is directed to the fabrication by ion implantation of monometallic and bimetallic Ag and Au particles in commercial soda-lime glass and to the optical and structural characterization of the obtained materials using high-resolution electron microscopy (HREM) in addition to TEM. In a first approach, the influences of

* Corresponding author. Tel.: +49 345 5525524; fax: +49 345 5527159.
E-mail address: manfred.dubiel@physik.uni-halle.de (M. Dubiel).

0022-3093/$ - see front matter © 2007 Elsevier B.V. All rights reserved.
doi:10.1016/j.jnoncrysol.2007.07.089

substrate temperature and implantation dose have been investigated for single Ag ion implantation.

2. Experimental procedures

Soda-lime glass containing (in mol%) 72.4% SiO_2, 14.4% Na_2O, 6.4% CaO, 6.0% MgO, 0.5% Al_2O_3, 0.20 K_2O, 0.3 SO_3 and 0.04% Fe_2O_3 were exposed to Ag^+ (200 keV), and/or to Au^+ (150 keV) ion implantation at 77 K, and at room temperature. On glass sheets of 1mm thickness areas of 20×10 mm^2 have been subjected to implantation for each type of ions at doses ranging from 0.5×10^{16} to 4×10^{16} ions/cm^2. The beam current density has been varied in the range of 0.5–2 μA/cm^2. Charge buildup reduction at the glass surface during implantation was achieved by electron beam irradiation onto the surface. The depth distribution of glass constituents and of the implanted ions was measured by Rutherford backscattering spectroscopy (RBS) using He^+ ions. To characterize the surface plasmon resonance due to the metal nanoparticles formed in the implanted areas the optical density of glass samples was recorded by means of a Perkin–Elmer spectrometer in the wavelength range of 250–900 nm.

Transmission electron microscopy examination to evaluate size, size distribution, and penetration depth of silver particles was done by means of a JEM 1010 operating at 100 kV. To this aim planar and cross-section preparation were applied including mechanical grinding, polishing and ion-beam etching. For advanced structural characterization a high-resolution electron microscope (HREM) operating at 400 kV (JEM 4010) was used. Lattice parameters of individual particles were determined from digitized HREM micrographs by image processing (real space and diffractogram evaluation) using the Digital Micrograph (GATAN) and NIH Image software [16]. For this evaluation only images of single crystalline particles have been considered which mostly displayed {111} and/or {200} lattice planes according to a face centered cubic structure.

3. Results

3.1. Ag single ion implantation

The evolution of absorption spectra shown in Fig. 1 for Ag^+ fluences between 5×10^{15} and 4×10^{16} ions/cm^2, with the beam current density set to 1 μA/cm^2 in all cases, exhibits considerable differences for different process temperatures. At 77 K it needs a distinctly higher dose ($>1 \times 10^{16}$ ions/cm^2) than at 295 K to induce measurable particle formation. Maximum position and full width at half maximum of the absorption band of the low temperature samples indicate the presence of extremely small Ag nanoparticles (<2 nm) of appreciable high concentration [17] while the corresponding parameters of the room temperature (RT) samples indicate the presence of distinctly larger nanoparticles [18].

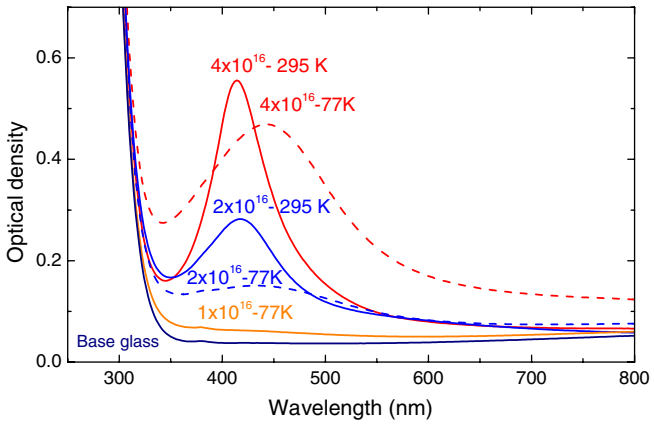

Fig. 1. Optical density of glasses implanted at various doses of Ag^+ ions/cm^2 performed at two different temperatures of 77 K (dashed lines) and 295 K (full lines).

As can be seen from TEM images of the RT sample shown in Fig. 2, with 2 μA/cm^2 beam current density Ag nanoparticles are formed even at the lowest implantation dose applied. From the cross-section micrographs it may be recognized that with increasing implantation dose the width of the particle layer beneath the glass surface increases. Simultaneously, the mean particle size is enhanced from ≈4.4 to ≈7.8 nm while the size distribution broadens considerably. From the size-dependent lattice plane spacings evaluated from HREM images (see inset in Fig. 2) almost no additional stress may be deduced.

3.2. Ag and Au double ion implantation

Based on the above findings sequential double ion implantations have been performed with Au^+ and Ag^+. A number of absorption spectra of glasses subjected to implantation of both ions of varying dose together with comparative spectra from single ion implantation are comprised in Fig. 3. From this figure it can be seen that for double ion implantation with 1 μA/cm^2 at RT the spectra are dominated by the absorption of Au nanoparticles having band maxima around 550 nm [19] and only at doses as high as 4×10^{16} ions/cm^2 for both metals a shift to a maximum position in between those of monometallic Ag and Au nanoparticles occurs. The shift of the peak maximum to about 570 nm for the 2×10^{16} Ag^+ plus 4×10^{16} Au^+ sample indicates that in this case silver ion implantation mainly results in the formation of larger particles [18] rather than contributing to alloy formation.

The cross-section TEM of the high-dose sample is shown in Fig. 4. Besides the finding that the particle layer of 135 nm thickness begins from the very surface of the glass it reveals the presence of extraordinary large nanoparticles in the center of this layer. The smaller nanoparticles are of ≈5 nm mean size, but the larger ones of ≈15 nm mean size have irregular image contrasts that point to the presence of central voids of considerable size. From the HREM image of one of the larger particles shown in

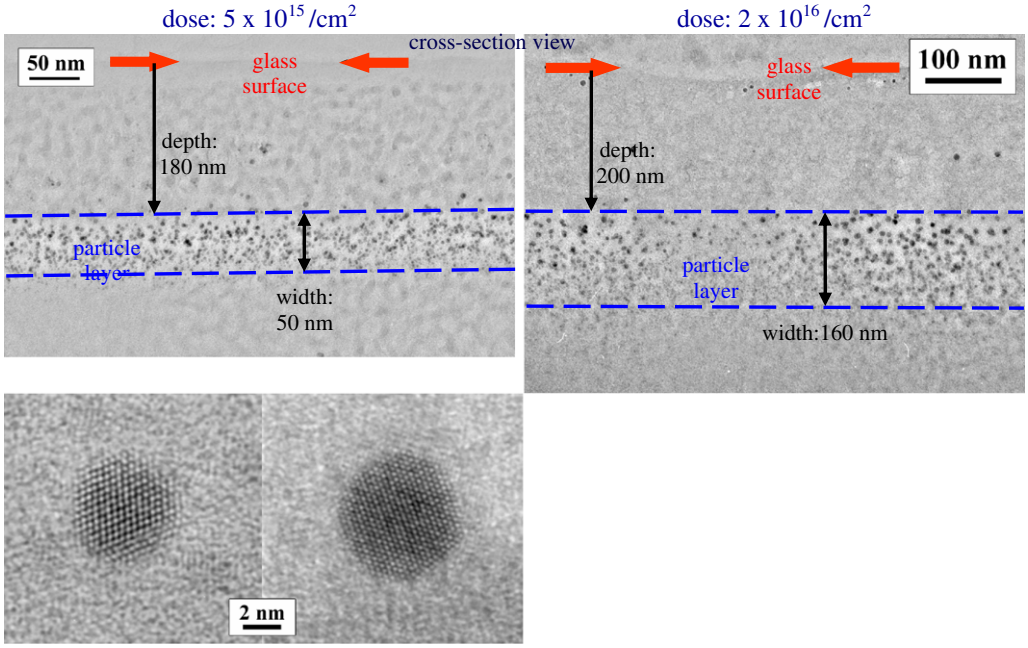

Fig. 2. Cross-section TEM image of glasses subjected to Ag^+ implantation at doses of 5×10^{16} and 2×10^{16} ions/cm^2; inhomogeneities in the particle layer are due to preparation effects (thickness variation). HREM lattice plane images of Ag nanoparticles are shown in the inset at the bottom.

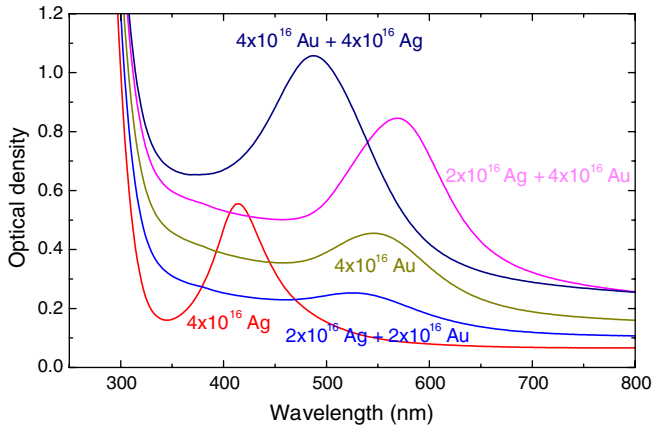

Fig. 3. Optical density of single Ag^+ or Au^+ and double implanted glasses at beam current density of 1 μA/cm^2 and at 295 K.

Fig. 5 one may clearly recognize the reduced contrast in its central region. The whole particle exhibits typical lattice plane fringes corresponding to a (1 1 0) zone axis orientation of a single-crystalline configuration.

4. Discussion

4.1. Effect of process temperature and dose

As already indicated by preceding studies [19,20] the present work verifies that the implantation dose and the beam current density influence strongly diffusion and precipitation processes as well as size and stress state of Ag nanoparticles formed. The low temperature inhibition of metal precipitation might be employed to achieve Ag doping of glass samples independent on subsequent thermally-induced particle formation. At increased doses of 2×10^{16}–4×10^{16} ions/cm^2 the input of collisional energy obviously suffices to generate Ag nanoparticles even at 77 K, although of rather small size. However, the shift of

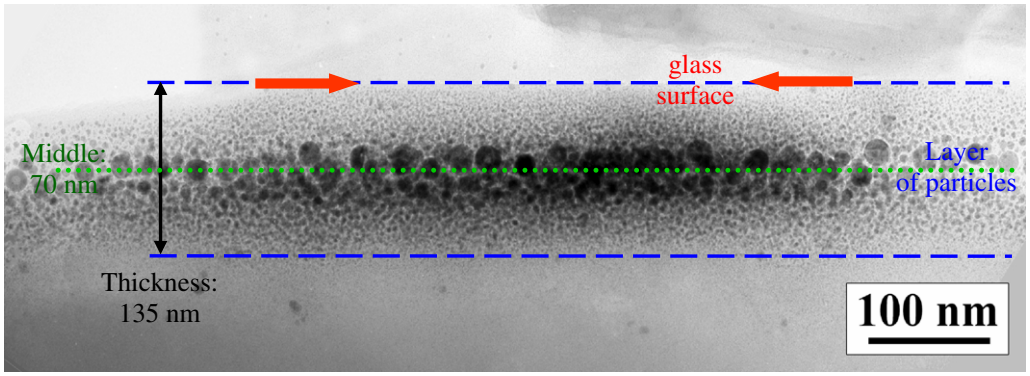

Fig. 4. Cross-section TEM image upon sequential implantation of 4×10^{16} Au^+ plus Ag^+ ions/cm^2 at beam current density of 1 μA/cm^2.

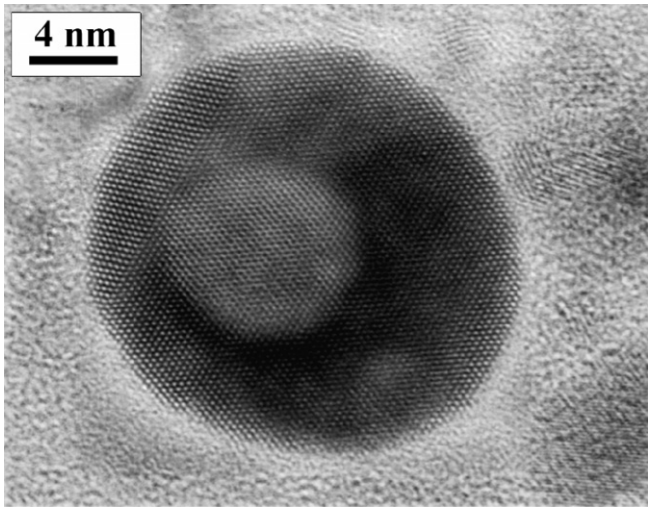

Fig. 5. HREM image of a void configuration in an Au–Ag nanoparticle upon implantation at doses of 4×10^{16} ions/cm^2 for each type of ions.

absorption maxima towards shorter wavelengths upon implantation at RT indicates a distinct increase of particle sizes. Consequently, the particles are attainable to TEM examination so as to evaluate extension of the particle layer and of the mean particle size. The particle size distribution always exhibits a non-Gaussian shape with asymmetric tail at larger sizes. These findings demonstrate that at RT the precipitation of implanted Ag ions to form crystalline Ag nanoparticles is nearly completed. At lower temperatures, however, a certain part of Ag species is assumed to remain in the ionic state as confirmed by EXAFS studies at the Ag K-edge of the Ag–O neighborhood.

4.2. Formation of alloy nanoparticles

The experimental results reveal that the formation of alloy Au/Ag particles could be achieved for high-dose implantation (4×10^{16} ions/cm^2 or more) of both, Ag^+ and Au^+ ions only. The evaluation of size-dependent lattice plane spacings from HREM images confirms that also upon double implantation nearly no additional stress is present in the particles. In particular, the lattice parameters determined for the fraction of larger particles agrees within the obtainable precision of about 1% to that of bulk Au or Ag (0.2355 nm or 0.2359 nm) being nearly the same. Consequently, also the lattice spacings of alloy nanoparticles should be the equal. The missing signature of alloy formation in the spectra of samples subjected to lower doses of double implantation may be discussed in terms of the well-known threshold of energy impact and sample heating required to achieve stable incorporation of a distinct fraction of the implanted Ag^+ into the nanoparticles formed [21]. Reports on the formation of Au–Ag alloy particles upon of 3×10^{16} ions/cm^2 double implantation in silica [12,13] did not mention any threshold, but instead an increase of the corresponding absorption upon subsequent annealing in air. This is different from the behavior of our double implanted glass samples where the alloy formation is assumed to be accompanied by complete reduction of the implanted ions present.

Although a definitive proof of a detailed void formation mechanism cannot yet be given, we assume that the image contrast features observed in larger alloy particles are due to a hollow nanoparticle configuration. This interpretation has been confirmed by preliminary studies using analytical transmission electron microscopy. Another example of void formation in nanoparticles has been found for sequential implantation of Cd^+ and S^- in silica [22]. Image contrast features comparable to those observed in our large alloy nanoparticles have been reported for sequential implantation of Ag^+ and Cu^+ in silica glass [23] and explained as a result of the aggregation of vacancies to nanovoids induced by irradiation. Accordingly, we assume the high energy impact accompanied by collision cascades during ion implantation to be responsible for the formation and aggregation of vacancies to nanovoids and their coalescence to larger cavities. Efforts are in progress now to confirm this assumption by additional experiments at various process temperatures.

5. Conclusion

The implantation of noble metal ions to form Ag nanoparticles, and Ag–Au nanoparticles in a surface-near region of commercial soda-lime glass has been studied for various process conditions. Ag^+ implantation at low temperatures has been found to cause an inhibition of the particle formation below a threshold dose, while at temperatures near RT a rather effective precipitation of the implanted Ag has been achieved for all doses applied. That should enable a better control of nucleation and growth processes involved in the nanoparticle formation using well-defined thermal processing and multiple implantation.

High-dose sequential implantation of Au^+ and Ag^+ resulted in the formation of Au–Ag alloy nanoparticles where the larger particles mostly exhibit an internal void configuration being caused by the ion implantation process. Although such configurations should influence the corresponding surface plasmon absorption band, it may be difficult to separate these effects from the absorption of the majority of smaller alloy particles.

Acknowledgement

This work has been supported by the Deutsche Forschungsgemeinschaft (SFB 418).

References

[1] P. Chakraborty, J. Mater. Sci. 33 (1998) 2235.
[2] F. Gonella, P. Mazzoldi, in: H.S. Nalwa (Ed.), Handbook of Nanostructured Materials and Nanotechnology, vol. 1, Academic, 2000, p. 81.
[3] P.D. Townsend, D.E. Hole, Vacuum 63 (2001) 641.

[4] D. Chakravorty, S. Basu, P.K. Mukherjee, S.K. Saha, B.N. Pal, S. Bhattacharya, J. Non-Cryst. Solids 352 (2006) 109.
[5] A.L. Stepanov, Rev. Adv. Mater. Sci. 4 (2003) 123.
[6] R.H. Magruder III, R.A. Zuhr, Nucl. Instr. and Meth. B 141 (1998) 256.
[7] K. Fukumi et al., J. Appl. Phys. 75 (1994) 3075.
[8] N. Toshima, T. Yonezawa, New J. Chem. XX (1998) 1179.
[9] R. Philip, G.R. Kumar, N. Sandhyarani, T. Pradepp, Phys. Rev. B 62 (19) (2000) 13160.
[10] S. Hannemann, J.-D. Grunwaldt, F. Krumeich, P. Kappen, A. Baiker, Appl. Surf. Sci. (2006).
[11] M. Mandal, N.R. Jana, S. Kundu, S.K. Ghosh, M. Panigrahi, T. Pal, J. Nanoparticle Res. 6 (2004) 53.
[12] G. Battaglin, E. Cattaruzza, F. Gonella, G. Mattei, P. Mazzoldi, C. Sada, X. Zhang, Nucl. Instr. and Meth. B 166&167 (2000) 857.
[13] F. Gonella et al., J. Non-Cryst. Solids 280 (2001) 241.
[14] G. Mattei, G. Battaglin, V. Bello, G. De Marchi, C. Maurizio, P. Mazzoldi, M. Parolin, C. Sada, J. Non-Cryst. Solids 322 (2003) 17.
[15] V. Bello, G. De Marchi, C. Maurizio, G. Mattei, P. Mazzoldi, M. Parolin, C. Sada, J. Non-Cryst. Solids (2004).
[16] W. Rasband, NIH Image' public domain software, US National Institute of Health (FTP: http://zippy.nimh.nih.gov).
[17] K.-J. Berg, A. Berger, H. Hofmeister, Z. Phys. D 20 (1991) 309.
[18] U. Kreibig, M. Vollmer, Optical Properties of Metal Clusters, in: Springer Series in Material Science, vol. 25, Berlin, Heidelberg, 1996.
[19] M. Dubiel, R. Schneider, H. Hofmeister, K.-D. Schicke, J.C. Pivin, Europ. Phys. J. D 43 (2007) 291.
[20] M. Dubiel, H. Hofmeister, E. Schurig, E. Wendler, W. Wesch, Nucl. Instr. and Meth. B 166&167 (2000) 871.
[21] A. Meldrum, R.F. Haglund, L.A. Boatner, C.W. White, Adv. Mater. 13 (2001) 1431.
[22] A. Meldrum, L.A. Boatner, C.W. White, R.C. Ewing, Mat. Res. Innovat. 2 (2000) 190.
[23] X. Xiao, C. Jiang, F. Ren, J. Wang, Y. Shi, Solid State Commun. 137 (2006) 362.